Tikrit Journal of Engineering Sciences

TJES Tikrit Journal of Engineering Sciences

Open Access

Article

# Optimal Controllers Design for Position Control of DC Servo Motor Under Disturbance

**Kareem A. Al-badri *, Rawaa R. Al-majeez**

Control and Systems Engineering Department, University of Technology, Baghdad, Iraq.

Emails:
Kareem A. Al-badri: 60186@uotechnology.edu.iq , Rawaa R. Al-majeez: 60188@uotechnology.edu.iq

## Abstract:

In this study, various optimized control schemes are designed to control the angular position of the DC servo motor (DCSM) system in the presence of an external torque disturbance. These control schemes include the optimized Proportional-Integral-Derivative (PID) controller, the optimized Synergetic Controller (SC), and the optimized Modified Sliding Mode Controller (MSMC). The optimal gains of these controllers have been determined using Particle Swarm Optimization (PSO). A comparative study has been conducted to assess the performance of the controlled system by using these optimal controllers to control the DCSM's angular position. To avoid falling into local optimal solutions, a modified version of the PSO technique is used. The numerical simulation results obtained with MATLAB reveal that the performance of the MPSO-based MSMC is superior to that of the PID and SC controllers in minimizing settling time, electric current quality, and fitness evaluation value under an external torque disturbance.

## Keywords:

Sliding-mode controller; synergetic controller; PID controller; particle swarm optimization technique; DC servo motor.

## Highlights:

- PID controller, SC, and MSMC are used and examined in the presence of an external torque disturbance for controlling the angular position of the DCSM system.
- The optimal gains of the proposed controllers are determined using the practical PSO approach with a modified version to avoid local optima.
- MSMC is superior to other control methods in terms of settling time reduction, current quality improvement, and fitness evaluation value enhancement under external torque disturbance, as demonstrated by MATLAB simulations.

## Citation:

Al-badri KA, Al-majeez RR. **Optimal Controllers Design for Position Control of DC Servo Motor Under Disturbance**. *Tikrit Journal of Engineering Sciences* 2026; **33**(1): 2206.

## Article History:

| | | | |
|---|---|---|---|
| Received: | 01 | Jun. | 2024 |
| Received in revised form: | 22 | Oct. | 2024 |
| Accepted: | 18 | Feb. | 2025 |
| Final Proofreading: | 19 | Apr. | 2026 |
| Available online: | 14 | May | 2026 |

https://doi.org/10.25130/tjes.33.1.20

Corresponding Author*:
**Kareem A. Al-badri**
Control and Systems Engineering Department/University of Technology /Baghdad, Iraq.
Email: 60186@uotechnology.edu.iq

## 1.INTRODUCTION

DC servomotors are electromechanical devices that allow precise control of angular position and motion in response to an applied input voltage. These devices are widely used in industrial applications that require high-dynamics in position and speed control, such as production lines, automatic machine tools, robotics, and computer peripherals. The reason for so many applications is the precise, wide, simple, and continuous control characteristics [1,2].The objective of this study is to control the angular position of the DCSM system in the presence of external torque disturbances, as the servo control system is the primary mechanism for movement in various industrial machinery. The precision of the machinery is primarily contingent upon the accuracy of the servo control system. Therefore, several modern control strategies have been proposed for the DCSM's angular position system. The following review of the most pertinent studies is presented hereafter. In Ref. [3], D. Mosconi, M. M. Da Silva, and A. A. G. Siqueira proposed a PID controller with the Fibonacci search method for controlling the DCSM angular position. A sliding-mode controller has been used to track the DCSM angular position by Durdu and Dursun [1]. Wang and Suh applied a unique wavelet-based nonlinear time-frequency control technique to simultaneously regulate the DC motor's position and speed [4]. Controlling the DCSM system's angular position was demonstrated by Priya and colleagues through implementing a fuzzy logic controller [5]. Rahman et al. [2] used a fractional transformation-based intelligent H-infinity controller to illustrate DCSM system position control. In another study [6], Xiang and Wei proposed LQR methods for the DCSM's angular position control. A compensation method combining fuzzy integral sliding mode and integral sliding mode has been introduced to control the angular position of the DCSM by Choudhary et al. [7]. Literature shows that robust and effective control features can be achieved by optimizing the modified sliding-mode control, particularly for this uncertain assistive system. Because setting gains via a trial-and-error approach is time-consuming and does not yield the ideal dynamic of the controlled system, the PSO technique is used to tune the suggested controllers' gains [8,9]. The following points summarize the contributions of this work:

- Developing sliding mode, synergetic, and PID control strategies to control the DCSM system's angular position.
- Developing the PSO algorithm to determine the gains of the proposed controllers and to improve the DCSM system's dynamic performance.

The remaining work is structured as follows: the mathematical equations of the DCSM system are presented in Section 2. The suggested controllers' design is illustrated in Section 3. Section 4 describes the PSO algorithm used to identify the ideal variables for the suggested controllers. The results of the computer simulations for the designed controllers are shown in Section 5. Lastly, section 6 provides the conclusions.

## 2.MATHEMATICAL MODEL

The equivalent circuit diagram and the dynamic model of the DCSM circuit are depicted in Fig. 1 and in Eqs. (1-7) [2,4]:

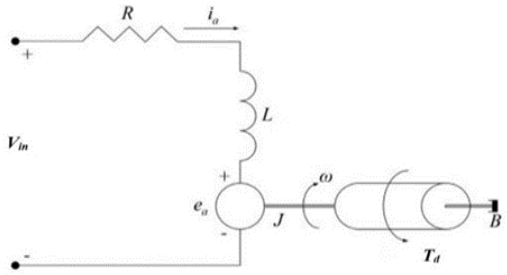


**Fig. 1** DCSM Equivalent Circuit [4].

This is how the electrical component of the DCSM is represented:

$$\boldsymbol{V_{in}(t) = Ri_a(t) + L\frac{di_a(t)}{dt} + e_a(t)} \qquad \textbf{(1)}$$

Where, $V_{in}(t)$ represents the input DC voltage,

$R$ represents the armature resistance, $L$ represents the armature inductance, $i_a(t)$ represents the armature current, and $e_a(t)$ represents the back electromotive force (emf). The back electromotive force is described in Eq. (2):

$$\boldsymbol{e_a(t) = K_b\dot{\theta}(t)} \qquad \textbf{(2)}$$

Where $k_b$ represents the back emf constant, $\dot{\theta}(t)$ and represents the motor's angular velocity. For $L \ll R$, the armature inductance can be ignored to simplify the system model. As a result, this is how the armature current is expressed:

$$\boldsymbol{i_a(t) = \frac{V_{in}(t)}{R} - \frac{k_b}{R}\dot{\theta}(t)} \qquad \textbf{(3)}$$

The motor electromagnetic torque is expressed as follows:

$$\boldsymbol{\tau_m(t) = k_t i_a(t)} \qquad \textbf{(4)}$$

Where, $k_t$ represents the torque coefficient.

The DCSM 's mechanical equation is represented as follows:

$$\boldsymbol{J\ddot{\theta}(t) + B\dot{\theta}(t) - T_d(t) = k_t i_a(t)} \qquad \textbf{(5)}$$

Where $J$ represents the motor inertia constant, $B$ represents the motor viscous-friction constant, $\dot{\theta}(t)$ represents the motor's angular velocity, $\ddot{\theta}(t)$ represents the motor's angular acceleration, and $T_d(t)$ and represents the external torque disturbance.

Eq. (6) is given by substituting Eq. (3) into Eq. (5) with some rearrangement as follows:

$$\ddot{\boldsymbol{\theta}}(\boldsymbol{t}) = -\left(\frac{\boldsymbol{RB+k_tk_b}}{\boldsymbol{JR}}\right)\dot{\boldsymbol{\theta}}(\boldsymbol{t}) + \frac{\boldsymbol{k_t}}{\boldsymbol{JR}}\boldsymbol{V_{in}}(\boldsymbol{t}) + \frac{\boldsymbol{T_d(t)}}{\boldsymbol{J}} \quad \textbf{(6)}$$

Let $x_1(t) = \theta(t)$ and $x_2(t) = \dot{\theta}(t)$, The following is a description of the state space representation:

$$\begin{bmatrix}\dot{\boldsymbol{x_1}}(\boldsymbol{t})\\ \dot{\boldsymbol{x_2}}(\boldsymbol{t})\end{bmatrix} = \begin{bmatrix}\boldsymbol{0} & \boldsymbol{1}\\ \boldsymbol{0} & -\left(\frac{\boldsymbol{RB+k_tk_b}}{\boldsymbol{JR}}\right)\end{bmatrix}\begin{bmatrix}\boldsymbol{x_1}(\boldsymbol{t})\\ \boldsymbol{x_2}(\boldsymbol{t})\end{bmatrix} + \begin{bmatrix}\boldsymbol{0}\\ \frac{\boldsymbol{k_t}}{\boldsymbol{JR}}\end{bmatrix}\boldsymbol{u}(\boldsymbol{t}) + \begin{bmatrix}\boldsymbol{0}\\ \frac{\boldsymbol{1}}{\boldsymbol{J}}\end{bmatrix}\boldsymbol{T_d}(\boldsymbol{t}) \quad \textbf{(7)}$$

## 3.CONTROLLERS DESIGN

In this section, a tracking control design for the DCSM angular position is proposed using three control techniques. The first technique uses the PID control method. The second technique is carried out based on the synergetic control method. The third solution is implemented using sliding-mode control. These three control techniques are initiated with the definition of the error $(e(t))$ as the difference between the actual and the desired angular positions as follows:

$$(\boldsymbol{t}) = \boldsymbol{x_1}(\boldsymbol{t}) - \boldsymbol{x_d}(\boldsymbol{t}) \quad \textbf{(8)}$$

Where $x_1(t)$ denotes the actual angular position, and $x_d(t)$ denotes the desired angular position.

In the first technique, the PID controller's control law combines three controller terms: proportional, integral, and derivative actions. As a result, Eq. (9) describes the control rule of the continuous-time PID controller [8,10]:

$$\boldsymbol{u}(\boldsymbol{t}) = \boldsymbol{Kpe}(\boldsymbol{t}) + \boldsymbol{Ki}\int \boldsymbol{e}(\boldsymbol{t}) + \boldsymbol{Kd}\frac{\boldsymbol{de(t)}}{\boldsymbol{dt}} \quad \textbf{(9)}$$

Where $e(t)$ is the error signal, $Kp$ is the proportional coefficient, $Ki$ is the integration coefficient, $Kd$ is the differentiation coefficient, and $u(t)$ is the control law.

The general block diagram for the controlled system using the MPSO-based PID controller is depicted in Fig.2. In the second technique, the control design is initiated by taking the 1st and 2nd derivatives of Eq. (8) to obtain Eqs. (10) and (11) as follows [11,12]:

$$\dot{\boldsymbol{e}}(\boldsymbol{t}) = \dot{\boldsymbol{x}}_1(\boldsymbol{t}) - \dot{\boldsymbol{x}}_d(\boldsymbol{t}) = \boldsymbol{x}_2(\boldsymbol{t}) - \dot{\boldsymbol{x}}_d(\boldsymbol{t}) \quad \textbf{(10)}$$

$$\ddot{\boldsymbol{e}}(\boldsymbol{t}) = \dot{\boldsymbol{x}}_2(\boldsymbol{t}) - \ddot{\boldsymbol{x}}_d(\boldsymbol{t}) \quad \textbf{(11)}$$

Where $x_2(t)$ is the actual velocity.

The macro-variable φ(e(t)) is described in Eq. (12) as follows:

$$\boldsymbol{\varphi}\big(\boldsymbol{e}(\boldsymbol{t})\big) = \boldsymbol{c_1e}(\boldsymbol{t}) + \dot{\boldsymbol{e}}(\boldsymbol{t}) \quad \textbf{(12)}$$

Where $c_1$ represents a scalar design parameter.

Taking the first derivative of Eq. (12) to obtain Eq. (13) as follows:

$$\dot{\boldsymbol{\varphi}}\big(\boldsymbol{e}(\boldsymbol{t})\big) = \boldsymbol{c_1}\dot{\boldsymbol{e}}(\boldsymbol{t}) + \ddot{\boldsymbol{e}}(\boldsymbol{t}) \quad \textbf{(13)}$$

The desired dynamic evolution of the macro-variables towards the manifold is described in Eq. (14).

$$\boldsymbol{T}\dot{\boldsymbol{\varphi}}\big(\boldsymbol{e}(\boldsymbol{t})\big) + \boldsymbol{\varphi}\big(\boldsymbol{e}(\boldsymbol{t})\big) = \boldsymbol{0} \quad \textbf{(14)}$$

Where $T > 0$ is the convergence rate of the macro-variables to the manifold $\varphi(e(t)) = 0$. This dynamic relies on ensuring that all trajectories of the state variables arrive at the intended manifold and remain there in the future. Eq. (16) is given by substituting Eq. (9)- Eq. (12) in Eq. (13) as follows:

$$\boldsymbol{T}(\boldsymbol{c_1}\dot{\boldsymbol{e}}(\boldsymbol{t}) + \ddot{\boldsymbol{e}}(\boldsymbol{t})) + \boldsymbol{\varphi}\big(\boldsymbol{e}(\boldsymbol{t})\big) = \boldsymbol{0} \quad \textbf{(15)}$$

$$\boldsymbol{Tc_1}\dot{\boldsymbol{e}}(\boldsymbol{t}) + \boldsymbol{T}\dot{\boldsymbol{x}}_2(\boldsymbol{t}) - \boldsymbol{T}\ddot{\boldsymbol{x}}_d(\boldsymbol{t}) + \boldsymbol{c_1}\big(\boldsymbol{x_1}(\boldsymbol{t}) - \boldsymbol{x_d}(\boldsymbol{t})\big) + \boldsymbol{x_2}(\boldsymbol{t}) - \dot{\boldsymbol{x}}_d(\boldsymbol{t}) = \boldsymbol{0} \quad \textbf{(16)}$$

To ensure that $T\dot{\varphi}(e(t)) + \varphi(e(t)) = 0$, the control law is designed as follows:

$$\boldsymbol{u}(\boldsymbol{t}) = \frac{\boldsymbol{JR}}{\boldsymbol{k_t}}\left(\left(\frac{\boldsymbol{RB+k_tk_b}}{\boldsymbol{JR}}\right)\boldsymbol{x}_2(\boldsymbol{t}) + \frac{\boldsymbol{T_d(t)}}{\boldsymbol{J}} - \boldsymbol{c_1}\big(\boldsymbol{x_2}(\boldsymbol{t}) - \dot{\boldsymbol{x}}_d(\boldsymbol{t})\big) + \ddot{\boldsymbol{x}}_d(\boldsymbol{t}) - \frac{\boldsymbol{c_1}(\boldsymbol{x_1}(\boldsymbol{t}) - \boldsymbol{x_d}(\boldsymbol{t})) + (\boldsymbol{x_2}(\boldsymbol{t}) - \dot{\boldsymbol{x}}_d(\boldsymbol{t}))}{\boldsymbol{T}}\right) \quad \textbf{(17)}$$

The general block diagram for the controlled system using the MPSO-based SC is shown in Fig. 3. In the third method, the sliding surface is defined as follows to begin the control design [13, 14]:

$$\boldsymbol{s}(\boldsymbol{t}) = \boldsymbol{\lambda e}(\boldsymbol{t}) + \dot{\boldsymbol{e}}(\boldsymbol{t}) \quad \textbf{(18)}$$

Where $s(t)$ is the sliding surface.

The equivalent control signal $u_e(t)$ can be obtained by taking the first derivative of Eq. (18) and setting it equal to zero. The discontinuous control signal $u_d(t)$ is symbolized as follows:

$$\boldsymbol{u_d}(\boldsymbol{t}) = -\boldsymbol{ksign}(\boldsymbol{s}) \quad \textbf{(19)}$$

Where $k$ is the discontinuous gain and $sign(s)$ is the sign function.

The chattering problem that appears in the classical sliding-mode control signal due to the signum function can be mitigated by using a boundary-layer function. Therefore, the saturation function (boundary layer function) is used instead of the signum function in the discontinuous control signal. As a result, the following can be expressed as the control signal of the modified sliding mode controller, which incorporates both the equivalent and discontinuous control signals:

$$\boldsymbol{u}(\boldsymbol{t}) = \frac{\mathbf{JR}}{\boldsymbol{K_t}}\left(\left(\frac{\boldsymbol{RB+K_tK_b}}{\boldsymbol{JR}}\right)\boldsymbol{x}_2(\boldsymbol{t}) + \frac{\boldsymbol{T_d(t)}}{\boldsymbol{J}} - \boldsymbol{\lambda x_2}(\boldsymbol{t}) - \boldsymbol{ksat}\big(\boldsymbol{s}(\boldsymbol{t})\big)\right) \quad \textbf{(20)}$$

The general block diagram of the controlled system using an MPSO-based MSMC is shown in Fig. 4.

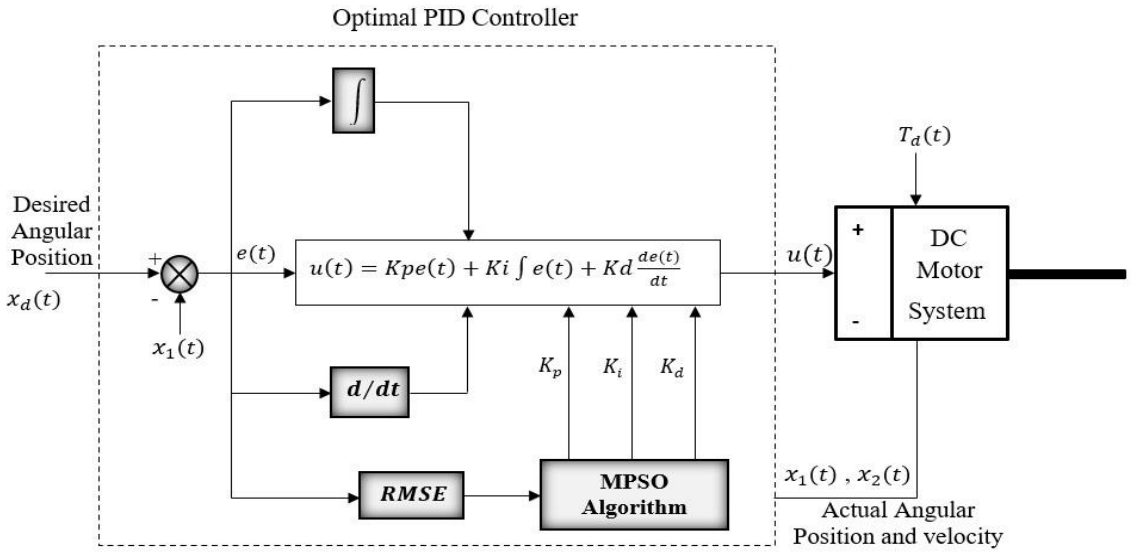


**Fig. 2** The Scheme of the Optimized PID Controller for the DCSM Model.

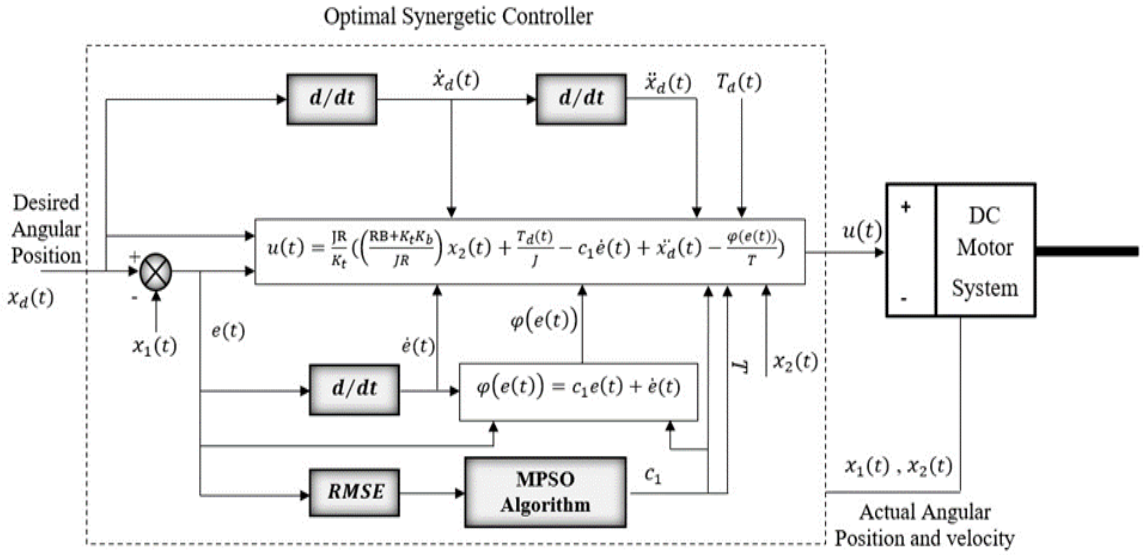


**Fig. 3** The Scheme of the Optimized SC for the DCSM Model.

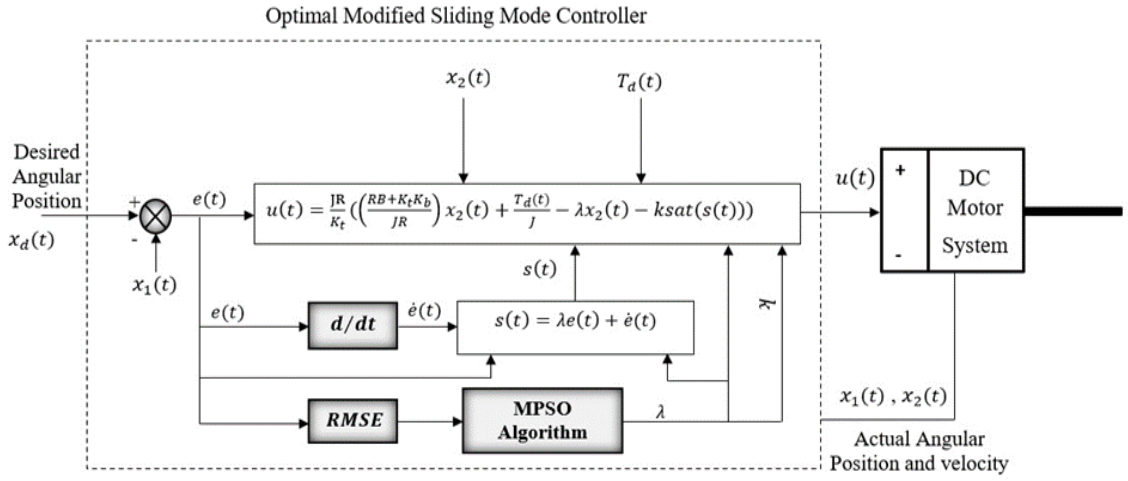


**Fig. 4** The Scheme of the Optimized MSMC Controller for the DCSM Model.

## 4.MPSO ALGORITHM

PSO is a heuristic technique for global optimization that was developed by Kennedy and Eberhart in 1995 and has since gained widespread popularity. This heuristic technique mimics the behavior of social behavior of birds within the flock to attain the target of food. Within the swarm, Particles interact with one another and learn from one another by using their locally best-seen solution as well as the swarm's globally best solution. A modified PSO algorithm can be used to avoid falling into local optimal solutions. In this algorithm, the velocity and position of the $i^{th}$ particle at $kk^{th}$ iteration are updated by utilizing the following equations [8, 15]:

$$V_i^{kk+1} = w_1 V_i^{kk} + c_o r_1 \left(p_{best_i}^{kk} - X_i^{kk}\right) + c_s r_2 \left(g_{\text{best}}^{kk} - X_i^{kk}\right) \quad (21)$$

$$X_i^{kk+1} = X_i^{kk} + V_i^{kk+1} \quad (22)$$

$$w_1 = w_{max} - kk(w_{max} - w_{min})/w_{max} \quad (23)$$

Where; $i = 1, 2, \dots, N_{pop}$, $\text{N}_{\text{pop}}$ denotes the population size, $kk = 1, 2, \dots, kk_{max}$, $kk_{max}$ denotes the maximum number of iterations, $V_i^{kk}$ denotes the $i^{th}$ particle's velocity at $kk^{th}$ iteration, $w_1$ represents the inertia factor, $c_o$ represents the cognitive weight, $c_s$ represents the social weight, $r_1$ and $r_2$ are random numbers between 0 and 1, $p_{best_i}^{kk}$ represents the personal best position found by the particle at $kk^{th}$ iteration, $g_{best}^{kk}$ represents the global best position found at $kk^{th}$ iteration by all particles, $w_{\text{max}}$ denotes the end value of the inertia factor, $w_{\text{min}}$ denotes the start value of the inertia factor, and $X_i^t$ represents the position of the $i^{th}$ bird at the $kk^{th}$ iteration.

The objective function selected to assess every particle during the search for the minimum in the search space is the Root Mean Square Error ($RMSE$). This objective function can be defined as follows [8]:

$$RMSE = \sqrt{\frac{1}{n}\sum_{i=1}^{n}(R - Z)^2} \quad (24)$$

Where n $n$ is the number of the required samples, $R$ is the reference signal, and $Z$ is the original signal.

The following pseudocode illustrates how the MPSO approach is used to adjust the gains of the suggested controllers:

**Pseudocode of the MPSO algorithm**

Step 1: Define Parameters.

(a) Define the parameters of the MPSO, including the end value of the inertia factor ($w_{\text{max}}$), the start value of the population size, the maximum number of iterations ($kk_{max}$), inertia factor ($w_{\text{min}}$), x and the maximum number of iterations ($kk_{max}$).

(b) for every particle $i = 1, \dots, N_p$, do

Set the particle's position and velocity at random initialization:

$V_i(0)$ and $X_i(0)$.

(c) For all particles, evaluate the cost function ($RMSE$) using Eq. (24).

(d) For all particles, assess $p_{best}$ to their initial position: $p_{best_i} = X_i(0)$.

(e) Place the $g_{best}$ value at the particle's location that has the lowest RMSE value out of all the particles.

end for

Step 2: Continue the operation until the maximum number of allowed iterations is reached.

While ($kk < kk_{max}$ ) do

for each particle $i = 1, 2, \dots, N_{pop}$, do

For each particle, change its velocity using Eq. (21).

For each particle, change its position using Eq. (22).

Evaluate the $RMSE_i$ function using Eq. (24).

if $\text{RMSE}\left(\text{X}_\text{i}^{\text{kk+1}}\right) < \text{RMSE}\left(\text{X}_\text{i}^{\text{kk}}\right)$.

$\text{p}_{\text{best}_\text{i}} = \text{X}_\text{i}^{\text{kk+1}}$.

end if

if $\min(\text{RMSE}(\text{X}^{\text{kk+1}}) < \min(\text{RMSE}(\text{X}^{\text{kk}})$

$\text{g}_{\text{best}} = \text{X}_{\text{min (RMSE)}}^{\text{kk+1}}$

end if

end for

$\text{kk} = \text{kk} + 1$

end while

Step 3: The optimal solution obtained is indicated by the output $g_{best}$ .

## 5.SIMULATION RESULTS

In this section, the efficacy of the suggested controllers has been assessed using MATLAB. The numerical values of the DCSM model and the optimal settings of the MPSO variables are shown in Tables 1 and 2, respectively [9]. A comparison study has been conducted to demonstrate the performance of the proposed optimal controllers with the presence of the external torque disturbance ($Td$), which equals (0.1 $N.m$) at the moment (6-7 $sec$). The desired angular position is described as variable steps of (1,2 and 3) radians, and the initial values of the variables $x_1$ and $x_2$ are set as follows:

$$[x_1(0), x_2(0)]^T = [0,0]^T.$$

Fig. 5 shows the objective function graphs for the controlled system utilizing the suggested optimal controllers for each MPSO technique iteration. The motor output angular position responses based on the proposed controllers are shown in Figs. 6 (a) and (b). It is evident that the output position response of the DCSM using the MPSO algorithm based on the MSMC is better than that of the other optimal controllers in terms of reducing the settling time and the effect of the external torque disturbance. The dynamic behavior of the controlled system using these optimal controllers and the optimal gains setting of the proposed controllers are described in Tables 3 and 4, respectively.

**Table 1** The Parameters of the DC Servo Motor System [9].

| Parameter | Value |
|---|---|
| $R$ | $5\,\Omega$ |
| $B$ | $0.136\ N.m.\ s$ |
| $k_t$ | $0.245\ N.m/A$ |
| $k_b$ | $0.245\ V.\ s/rad$ |
| $J$ | $0.0025\ kg.\ m^2/s^2$ |
| $L$ | $0.01\ H$ |

**Table 2** The Parameters Used in the MPSO Algorithm.

| Parameter | Value |
|---|---|
| Population size | 30 |
| Maximum number of iterations | 100 |
| Cognitive parameter | 1.49618 |
| Social parameter | 1.49618 |
| Maximum and minimum values of inertia weight | 0.9, 0.1 |
| The dimension of the problem | 3 for PID controller<br>2 for SC<br>2 for SMC |

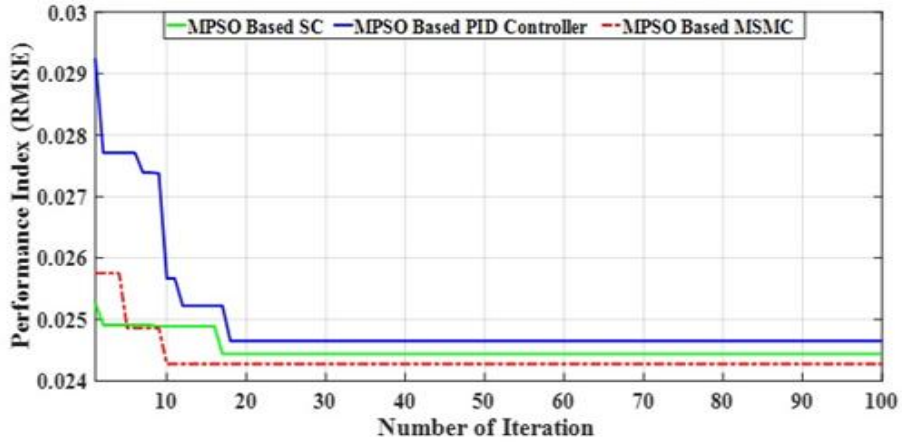


**Fig. 5** The Behavior of the Suggested Controllers' Cost Function (RMSE).

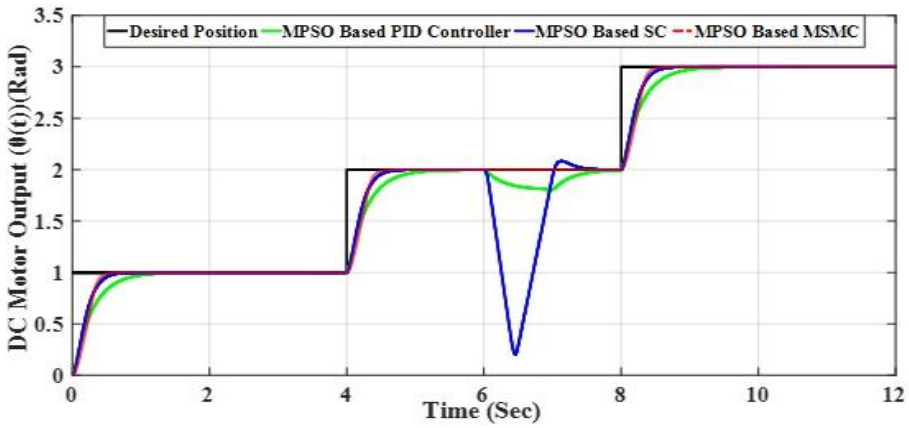


**(a)**

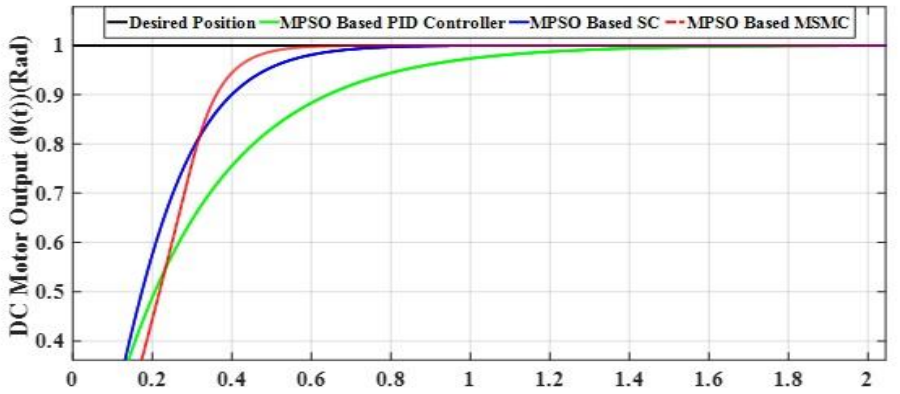


**(b)**

**Fig. 6** (a) The Controlled System Angular Position Response Using the Proposed Optimal Controllers, (b) A Zoomed- in View of the Angular Position Response.

**Table 3** Dynamic Response of the Controlled System Based on the Proposed Controllers.

| Controller | Settling Time (sec) | RMSE |
|---|---|---|
| MPSO-based PID controller | 1.6 | 0.024665 |
| MPSO based SC | 0.9 | 0.024448 |
| MPSO based MSMC | 0.6 | 0.024275 |

**Table 4** The Optimal Parameters of the Proposed Controller-Based MPSO Technique.

| Controller | Coefficient | Value |
|---|---|---|
| MPSO-based PID controller | $Kp$ | 10.438 |
| | $Ki$ | 0.00052 |
| | $Kd$ | 0.00027 |
| MPSO based SC | $c_1$ | 10.185 |
| | $T$ | 0.1085 |
| MPSO based MSMC | $\lambda$ | 15.021 |
| | $k$ | 2.506 |

Figures 7 and 8 show the angular velocity and the armature current responses of the controlled system using the proposed controllers, respectively. These figures show that the MPSO-based MSMC is faster and consumes less current than the other optimal controllers. In addition, the MPSO-based MSMC and MPSO-based PID controllers exhibit better responses than the MPSO-based SC under an external torque disturbance. Figure 9 shows the responses of the suggested optimal controllers to the voltage-control attempts. This figure demonstrates that these control attempts are smooth without oscillation response, do not display spike behavior, and fall within the permitted range of (12) volts, contingent upon the DCSM's supply voltage. Additionally, in terms of mitigating the impact of an external torque disturbance, the voltage control signals of the MPSO-based PID controller and MSMC perform better than those of the MPSO-based SC.

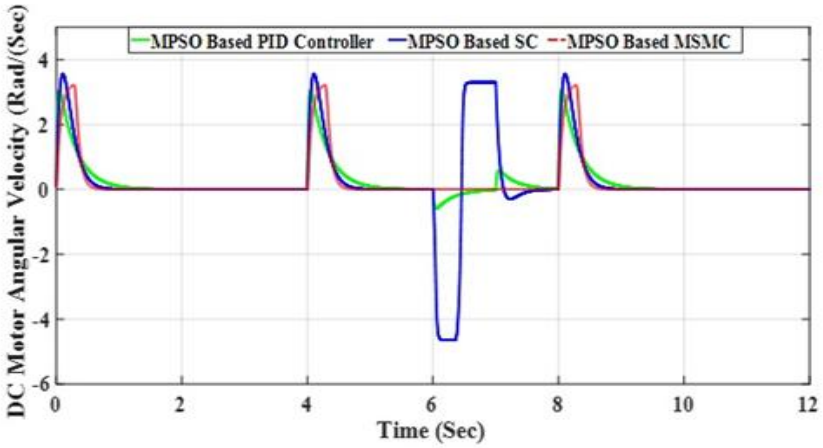


**Fig. 7** The Controlled System Angular Velocity Response Using the Proposed Optimal Controllers.

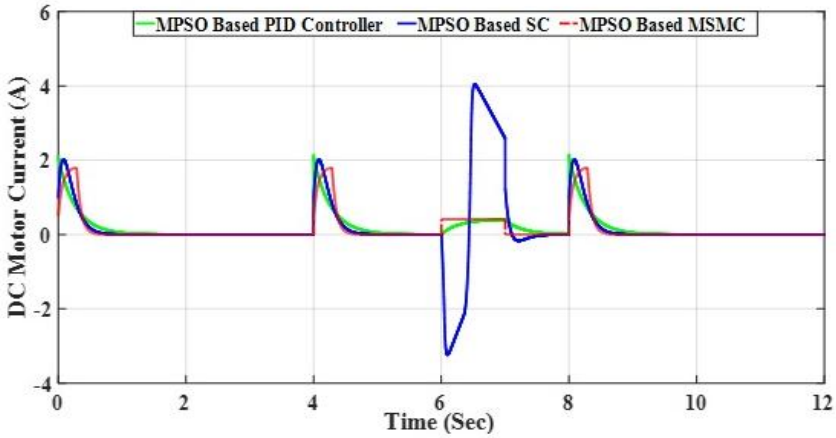


**Fig. 8** The Controlled System Armature Current Response Using the Proposed Optimal Controllers.

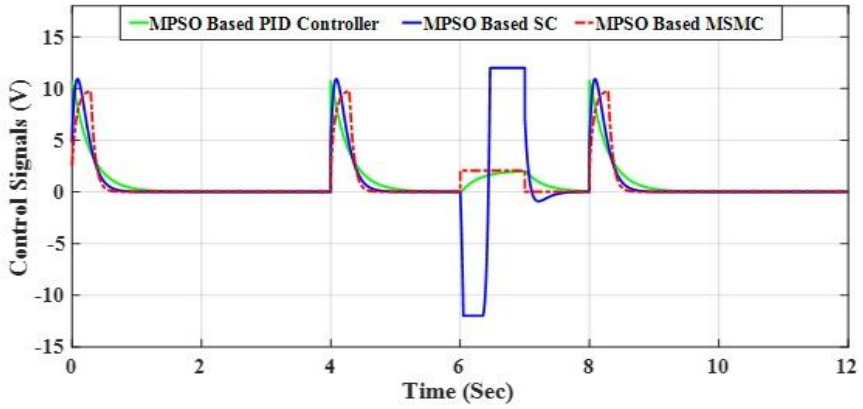


**Fig. 9** The Controlled System Voltage Control Signal Response Using the Proposed Optimal Controllers.

## 6.CONCLUSIONS

To manage the angular position of DCSM in the presence of external torque disturbances, this work presents different controller designs, including MPSO-based PID control, MPSO-based SC, and MPSO-based MSMC. The choice of parameters for these controllers is left to the MPSO approach. A comparison of the MPSO-based PID controller, MPSO-based SC, and MPSO-based MSMC has been done. The efficiency of the suggested controllers in reducing the system output's position-tracking error was demonstrated through computer simulation. The simulation results for the controlled system employing the MPSO-based MSMC indicated significant reductions in settling time of 33.333% and 62.5%, respectively, compared with the MPSO-based SC and MPSO-based PID controller. Additionally, the MPSO-based MSMC has reduced the controlled system's consumed electric current by 10% and 14.3%, respectively, compared to the MPSO-based SC and MPSO-based PID controller. Ultimately, the fitness evaluation value of the managed system employing the MPSO-based MSMC has dropped when compared to the MPSO-based SC and MPSO-based PID controller. For further work, this study can be extended by implementing the proposed control strategies in real-time environments to control the system, both with and without load, using embedded hardware such as FPGAs or LabVIEW. Another extension of this study is to use different control techniques to maintain the angular position of the DCSM system in the presence of external torque disturbances. A performance comparison can be conducted between these control strategies and the proposed controllers [16-25].

## ACKNOWLEDGEMENTS

The authors express their sincere gratitude to the Department of Control and Systems Engineering at the University of Technology, Iraq, for their support in this study. Furthermore, they acknowledge that all research expenses were self-funded, and their commitment ensured the successful completion of the research.

## REFERENCES

**[1]** Durdu A, Dursun EH. **Sliding Mode Control for Position Tracking of Servo System with a Variable Loaded DC Motor.** *Elektronika Ir Elektrotechnika* 2019; **25**(4): 8–16.

**[2]** Rahman MZU, Leiva V, Martin-Barreiro C, Mahmood I, Usman M, Rizwan M. **Fractional Transformation-Based Intelligent H-infinity Controller of a Direct Current Servo Motor.** *Fractal and Fractional* 2023; **7**(1): 29.

**[3]** Mosconi D, Silva MM, Siqueira AAG. **Optimal Tuning of a Proportional Controller for DC Motor Position Control via Fibonacci Search Method.** *Journal of Mechatronics Engineering* 2021; **4**(1): 12–21.

**[4]** Wang X, Suh CS. **Precision Concurrent Speed and Position Tracking of Brushed DC Motors Using Nonlinear Time-Frequency Control.** *Journal of Vibration and Control* 2017; **23**(19): 3266–3291.

**[5]** Priya J, Jeevanandham A, Rajalashmi K. **Fuzzy Logic Controller for Position Control of Servo Motor.** *International Journal of Innovative Technology and Exploring Engineering* 2019; **8**(3): 99–102.

**[6]** Xiang Z, Wei W. **Design of DC Motor Position Tracking System Based on LQR.** *Journal of Physics: Conference Series* 2021; **1887**(1): 012022.

**[7]** Choudhary K, Qureshi MS, Singh B. **Position Control of DC Servo Motor Using Improved Sliding Mode Control Techniques.** *International Journal of Applied Engineering Research* 2018; **13**(8): 15–19.

**[8]** Mohamed MJ, Rasheed LT. **Design of Nonlinear PID and FOPID Controllers for Electronic Throttle Valve Plate's Position.** *Journal of*

*Electrical and Computer Engineering* 2024; **2024**: 9984750.

**[9]** Rasheed LT. **Optimal Tuning of Linear Quadratic Regulator Controller Using Ant Colony Optimization Algorithm for Position Control of a Permanent Magnet DC Motor.** *Iraqi Journal of Computer, Communication, Control and System Engineering* 2020; **20**(3): 29–41.

**[10]** Mansoor AZ, Salih TA, Abdullah FS. **Speed Control of Separately Excited D.C. Motor Using Self-Tuned Parameters of PID Controller.** *Tikrit Journal of Engineering Sciences* 2013; **20**(1): 1–9.

**[11]** Humaidi AJ, Ibraheem IK, Azar AT, Sadiq ME. **A New Adaptive Synergetic Control Design for Single Link Robot Arm Actuated by Pneumatic Muscles.** *Entropy* 2020; **22**(7): 723.

**[12]** Mahdi SM, Yousif NQ, Oglah AA, Sadiq ME, Humaidi AJ, Azar AT. **Adaptive Synergetic Motion Control for Wearable Knee-Assistive System: A Rehabilitation of Disabled Patients.** *Actuators* 2022; **11**(7): 176.

**[13]** Sadiq ME, Humaidi AJ, Kadhim SK, Al Mhdawi A, Alkhayyat A, Ibraheem IK. **Optimal Sliding Mode Control of Single Arm PAM-Actuated Manipulator.** *11th International Conference on System Engineering and Technology (ICSET)* 2021; Shah Alam, Malaysia: 84–89.

**[14]** Al-Qassar AA, Al-Dujaili AQ, Hasan AF, Humaidi AJ, Ibraheem IK, Azar AT. **Stabilization of Single-Axis Propeller-Powered System for Aircraft Applications Based on Optimal Adaptive Control Design.** *Journal of Engineering Science and Technology* 2021; **16**(3): 1851–1869.

**[15]** Wali SA, Muhammed AK. **Power Sharing and Frequency Control in Inverter-Based Microgrids.** *Tikrit Journal of Engineering Sciences* 2022; **29**(3): 70–81.

**[16]** Husain SS, MohammadRidha T. **Integral Sliding Mode Controlled ATMD for Buildings under Seismic Effect.** *International Journal of Safety and Security Engineering* 2022; **12**(4): 413–420.

**[17]** Al-Ani FR, Lutfy OF, Al-Khazraji H. **Optimal Backstepping and Feedback Linearization Controllers Design for Tracking Control of Magnetic Levitation System: A Comparative Study.** *Journal of Robotics and Control* 2024; **5**(6): 1888–1896.

**[18]** Husain SS, Rasheed LT, Mahmod RA, Hamza EK, Noaman NM, Humaidi AJ. **Design of RISE Control for Respiratory System.** *8th International Conference on Engineering Technologies and Applied Sciences (ICETAS)* 2023; Bahrain: 1–5.

**[19]** Al Mhdawi AK, Wright N, Humaidi AJ, Azar AT. **Adaptive PI-Fuzzy Like Control of a Stack Pneumatic Actuators Testbed for Multi-Configuration Small Scale Soft Robotics.** *International Conference on Manipulation, Automation and Robotics at Small Scales (MARSS)* 2023; Abu Dhabi, United Arab Emirates: 1–8.

**[20]** Hamzah MK, Raafat SM, Al-Samarraie SA. **Boundary Layer-Based Event-Triggered Sliding Mode Controller for Nonlinear Systems with Uncertainty.** *Mathematical Modelling of Engineering Problems* 2024; **11**(6): 1505–1519.

**[21]** Kadhim MQ, Yaseen FR, Al-Khazraji H, Humaidi AJ. **Application of Terminal Synergetic Control Based Water Strider Optimizer for Magnetic Bearing Systems.** *Journal of Robotics and Control* 2024; **5**(6): 1973–1979.

**[22]** Mahmood NS, Humaidi AJ, Al-Azzawi RS. **Nonlinear PD State Feedback Control for Electronic Throttle Valve Based on Ant Colony Optimization.** *11th Conference on Systems, Process & Control (ICSPC)* 2023; Malacca, Malaysia: 38–43.

**[23]** Hameed AH, Al-Samarraie SA, Humaidi AJ. **Ultimate Bounded Observer-Based Control of Electrical Vehicle Driven by DC Motor System with Unmatched Load Torque.** *Advances in Mechanical Engineering* 2024; **16**(10): 1–14.

**[24]** Raheem RS, Hassan MY, Kadhim SK. **Particle Swarm Optimization Based Interval Type 2 Fuzzy Logic Control for Motor Rotor Position Control of Artificial Heart Pump.** *Indonesian Journal of Electrical Engineering and Computer Science* 2022; **25**(2): 814–824.

**[25]** Mohamed JM, Oleiw BK, Azar AT, Mahlous AR. **Hybrid Controller with Neural Network PID/FOPID Operations for Two-Link Rigid Robot Manipulator Based on the Zebra Optimization Algorithm.** *Frontiers in Robotics and AI* 2024; **11**: 1386968.